THE JOURNAL OF CHEMICAL PHYSICS **146**, 052807 (2017)

CrossMark
click for updates

Influence of C_{60} co-deposition on the growth kinetics of diindenoperylene–From rapid roughening to layer-by-layer growth in blended organic films

C. Lorch,[1] J. Novák,[1,2,3] R. Banerjee,[1,4] S. Weimer,[1] J. Dieterle,[1] C. Frank,[1] A. Hinderhofer,[1] A. Gerlach,[1,a)] F. Carla,[5] and F. Schreiber[1]

[1]*Universität Tübingen, Institut für Angewandte Physik, Auf der Morgenstelle 10, 72076 Tübingen, Germany*
[2]*Central European Institute of Technology, Masaryk University, Kamenice 5, CZ-62500 Brno, Czech Republic*
[3]*Department of Condensed Matter Physics, Faculty of Science, Masaryk University, Kotlarska 2, CZ-611 37 Brno, Czech Republic*
[4]*Department of Physics, Indian Institute of Technology Gandhinagar, Palaj, Gandhinagar 382355, India*
[5]*ESRF-The European Synchrotron, 71 Avenue des Martyrs, 38000 Grenoble, France*

(Received 28 July 2016; accepted 7 October 2016; published online 7 November 2016)

We investigated the growth of the two phase-separating materials diindenoperylene (DIP) and buckminsterfullerene C_{60} with different mixing ratio in real-time and *in situ* by X-ray scattering experiments. We found that at room temperature, mixtures with an excess of DIP show a growth mode which is very close to the perfect layer-by-layer limit with DIP crystallites forming over the entire film thickness. An unexpected increase in the island size is observed for these mixtures as a function of film thickness. On the other hand, equimolar and C_{60} dominated mixtures grow with poor crystallinity but form very smooth films. Additionally, it is observed that higher substrate temperatures lead to an increase in the length scale of phase separation with film thickness. *Published by AIP Publishing.* [http://dx.doi.org/10.1063/1.4966583]

INTRODUCTION

During the last years, devices fabricated with organic semiconductors (OSCs) have evolved to an attractive alternative to conventional inorganic ones. Organic electronics benefit from potentially low preparation costs, low-temperature processing, and flexible substrates.[1–8] OSCs can be employed as active layers in organic field effect transistors, organic light emitting diodes, or organic photovoltaics (OPVs).[9] For all of these devices, the crystallinity of the thin films, interface morphology as well as the orientation of the individual molecules is of substantial importance for the performance.[10,11] Particularly in the case of OPV, mixtures of two different materials can be employed as an active layer[12] and the mixing behavior and the associated length scales of the two materials play an important role. In general, various complex scenarios are possible. In a simple picture, one can distinguish between a statistical intermixing, an ordered crystal structure, or phase separation of the materials.[13–15] Obviously, in non-ideal cases the observed scenario may consist of a combination of these limiting cases. The observed mixing behavior depends on many parameters like the substrate temperature, deposition rate, mixing ratio, and sterical compatibility. Recently, for equimolar mixtures of the rod-like diindenoperylene (DIP) and the sphere-like buckminsterfullerene C_{60}, we reported a kinetically limited thickness-dependent phase separation.[16] Furthermore, this material combination has shown promising characteristics in OPV cells, employing planar heterojunction as well as bulk heterojunction geometries,[17] making it interesting for further investigations, while the growth of the pure materials on various substrates was studied in detail.[18–20]

In order to monitor the growth, to identify transient effects, and to exclude the influence of ambient conditions on the film structure, real-time *in situ* experiments are necessary. While scanning imaging methods like atomic force microscopy and scanning tunneling microscopy can reveal the local morphology in great detail, scattering techniques give non-invasive access to information on the nano-scale, statistically averaged over a much larger sample area[21–23] at higher probing frequencies for real-time experiments.[24,25] Real time monitoring of the scattering intensity at the anti-Bragg[26,27] point during the thin film growth allows to discriminate between the three basic growth modes:[28] the step-flow, the layer-by-layer, and three-dimensional (i.e., growth accompanied by the formation of islands higher than one mono-layer) growth modes, which result in constant scattered intensity, periodic intensity oscillations, and steep intensity decay, respectively. In the anti-Bragg regime, various probes including specular reflected thermal energy He atoms,[28] high energy electron diffraction (RHEED),[29,30] and X-ray reflection in the anti-Bragg point[26,31–35] have been used to follow the growth mode and detect growth instabilities. Additional information on atomic or molecular island density evolution, which may exhibit oscillations due to island nucleation and coalesce during growth, can be obtained by monitoring diffuse (off-specular) X-ray scattering.[36,37] The diffuse scattering can be detected for *in situ* experiments

a)Author to whom correspondence should be addressed. Electronic mail: alexander.gerlach@uni-tuebingen.de

Reuse of AIP Publishing content is subject to the terms: https://publishing.aip.org/authors/rights-and-permissions. Downloaded to IP: 134.2.183.35 On: Tue, 08 Nov 2016 10:24:20

in real time,[20,38–40] thanks to the advent of modern two dimensional X-ray detectors. Information obtained from the evolution of the diffuse scattering is complementary to that from the intensity evolution at the anti-Bragg point and it is important for an unambiguous interpretation of reciprocal space data.

We investigated the influence of substrate temperature and mixing ratio on the kinetics of the phase separation. We used various X-ray scattering techniques, namely X-ray reflectivity (XRR) and grazing incidence X-ray diffraction (GIXD), for probing the out-of-plane and in-plane film structure, respectively. Additionally, we follow in parallel the real time evolution of the diffuse scattering and of the intensity in the anti-Bragg point in a grazing incidence small angle X-ray scattering (GISAXS) geometry.[41,42] At higher substrate temperatures, the crystallinity of the pure phases as well as the length scale of phase separation increases with higher substrate temperatures. For mixtures with an excess of DIP, we observe an increase in the coherently scattering in-plane domain size $D_{coh\parallel}$ and the averaged island distance D_{island}. Furthermore, a near perfect layer-by-layer growth mode is observed for the DIP:C_{60} mixed film in the mixing ratio of 3:1. Contrary to this, for equimolar and C_{60} dominated mixtures the crystallinity of the films is significantly lower, although very smooth films are observed.

EXPERIMENTAL

DIP was obtained from the University of Stuttgart and purified twice via temperature gradient sublimation before use. C_{60} was purchased from CreaPhys and used without further purification. The films were prepared and investigated during growth in a portable ultrahigh vacuum chamber.[43] Silicon covered with native oxide (nSiO) was used as a substrate. The oxide layer thickness was approximately 2.7 nm. Before installation, the substrates were ultrasonically cleaned with acetone, isopropanol, and purified water. Before each film deposition, the substrate was heated up to 770 K. The pressure in the vacuum chamber was lower than 1×10^{-8} mbar during the deposition. Real-time GIXD measurements at the ID03 beamline of the ESRF were performed for films with mixing ratios DIP:C_{60} 1:1, 3:1, and 1:3 at substrate temperatures of 303 K, 338 K, and 373 K (no 1:1 at 338 K). The total growth rate was between 0.17 and 0.22 nm/min. The energy was set to 11.5 keV (corresponding to a wavelength of 1.08 Å). A MaxiPix area detector was employed and slits were put directly in front of the detector to mimic a point detector for real-time and postgrowth scans (XRR and wide-range GIXD). The XRR data were fitted using Parratt's formalism[44] implemented in the GenX software[45] up to $q_z = 0.20$ Å^{-1} using a model consisting of one bilayer, representing the wetting layer (i.e., completely filled molecular layers and partially filled molecular layers on the top which represent the wedding-cake like growth reported for DIP[46,47]). The Bragg peaks in the GIXD data were fitted with Gaussians to obtain the full width at half maximum (FWHM) of the peaks. Scherrer's equation ($D_{coh\parallel} = 2\pi K/\mathrm{FWHM}$ with $K = 0.94$ for spherical crystallites) was used to calculate $D_{coh\parallel}$.[48] The instrumental broadening was not included, hence the estimated values are lower limits only.

Real-time *in situ* GISAXS measurements were performed at the X04SA beam-line of the Swiss Light Source[49] at a wavelength of 1.00 Å. The incidence angle of the X-ray beam was fixed at $\alpha_i = 0.848°$, which corresponds to the anti-Bragg point of the DIP (0 0 1) out-of-plane reflection, and the scattered signal was detected using a PILATUS II two dimensional detector. Films of DIP:C_{60} 3:1, 2:1, 1:1, and 1:3 mixtures and the pure materials at 303 K substrate temperature were prepared.

RESULTS AND DISCUSSION

X-ray reflectivity

XRR measurements were performed to study the crystal structure perpendicular to the surface. Figure 1 depicts the data visually grouped according to the three different substrate temperatures 303 K, 338 K, and 373 K. Within each data group, the DIP:C_{60} 3:1 mixture is shown at the top with red circles, followed by the 1:1 (black empty triangles) and 1:3 (blue filled squares) mixtures, respectively. The pronounced Kiessig oscillations (in the range $q_z = 0.3$ Å^{-1}) are a strong indication for films with a smooth top surface. With increasing substrate temperature, these oscillations are more strongly attenuated due to higher surface roughness. The thickness and roughness extracted from fitting the data are summarized in Table I.

The thicknesses of the films extracted from the electron-density profiles differ by up to 25% from each other. Therefore, under the approximation of linear roughening, we compare the ratio σ/d (Table I). We can identify a much stronger roughening for the high T films (373 K) compared to the low T (303 K) films for all mixing ratios.

The black solid and red dashed vertical lines in Fig. 1 mark the Bragg peak positions of pure DIP and C_{60}, respectively. All

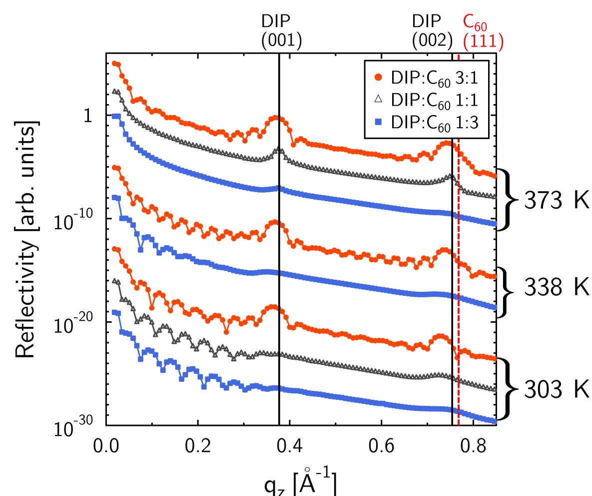

FIG. 1. XRR data of a sample series A. At substrate temperatures of 373 K (top), 338 K (middle), and 303 K (bottom), films with the mixing ratios DIP:C_{60} 3:1 (red filled circles), 1:1 (black empty triangles), and 1:3 (blue filled squares) were measured. The vertical lines indicate the Bragg positions for pure DIP (solid black) and C_{60} (dashed red) thin films. The curves are vertically shifted for clarity. Reprinted with permission from Ref. 66.

Reuse of AIP Publishing content is subject to the terms: https://publishing.aip.org/authors/rights-and-permissions. Downloaded to IP: 134.2.183.35 On: Tue, 08 Nov 2016 10:24:20

TABLE I. Summary of the film parameters extracted from the fitted XRR and GIXD data. The following values are listed: Substrate temperature T_{sub}, mixing ratio DIP:C_{60}, film thickness d, roughness σ, relative roughness σ/d, and in-plane coherent crystallite size $D_{coh\|}$ for DIP and C_{60}.

					$D_{coh\|}$ (nm)	
T_{sub} (K)	DIP:C_{60}	d (nm)	σ (nm)	σ/d	C_{60}	DIP
303	3:1	14.9 ± 0.2	1.4 ± 0.2	0.094 ± 0.013	4.7 ± 0.3	7.1 ± 0.3
303	1:1	13.2 ± 0.2	1.2 ± 0.2	0.091 ± 0.015	2.6 ± 0.2	N.A.
303	1:3	11.8 ± 0.2	1.2 ± 0.2	0.102 ± 0.017	4.1 ± 0.3	N.A.
338	3:1	17.8 ± 0.2	1.3 ± 0.2	0.073 ± 0.011	2.9 ± 0.2	12.6 ± 0.5
338	1:3	12.4 ± 0.2	1.8 ± 0.3	0.145 ± 0.024	3.7 ± 0.2	N.A.
373	3:1	16.0 ± 0.3	2.5 ± 0.3	0.156 ± 0.019	5.7 ± 0.4	20.5 ± 0.9
373	1:1	16.3 ± 0.5	4.1 ± 0.4	0.252 ± 0.026	7.6 ± 0.5	23.4 ± 0.9
373	1:3	16.5 ± 0.5	2.5 ± 0.5	0.152 ± 0.025	6.8 ± 0.5	20.1 ± 0.9

observed out-of-plane Bragg peaks can be clearly associated with one or the other compound. Since no other Bragg peaks are observed, it is obvious that the two materials form phase-separated crystalline domains, consisting of pristine materials, and no new hybrid crystal phase is observed. For all three different substrate temperatures, in the DIP:C_{60} 3:1 mixtures (red circles), the Bragg peaks (first and second order), which can be ascribed to standing-up domains of DIP, are clearly visible. For the same mixing ratio, the C_{60} (1 1 1) Bragg peak is observed only as a small hump on the high q_z side of the DIP (0 0 2) Bragg reflection. For mixtures with an excess of C_{60}, independent of the substrate temperature, no well-defined Bragg peaks can be observed, only at 373 K the DIP (0 0 1) reflection is slightly visible. For an equimolar mixing ratio, the substrate temperature has a relatively strong impact on the out-of-plane crystallinity. The DIP Bragg peaks get more pronounced with increasing substrate temperature. For all temperatures, the equimolar mixtures do not show any out-of-plane Bragg peaks corresponding to C_{60}. However, the out-of-plane coherent crystal size of the equimolar mixture at the highest temperature (373 K) is still smaller than the one of the DIP:C_{60} 3:1 mixture at 303 K.

Furthermore, the DIP Bragg peaks in mixtures grown at 303 K and 338 K are slightly shifted to lower q_z values, compared to pure DIP films.[50] The first (second) DIP Bragg peak is observed at 0.363 $Å^{-1}$ (0.729 $Å^{-1}$) and 0.368 $Å^{-1}$ (0.737 $Å^{-1}$) for 303 K and 338 K, respectively. At 373 K, the values are very close to the ones reported (0.371 $Å^{-1}$ and 0.742 $Å^{-1}$). This shift corresponds to an increase of the lattice vector perpendicular to the surface by 0.3 Å to 16.9 Å at a substrate temperature of 303 K compared to 16.6 Å in pure films or high T (373 K) mixtures. This increased out-of-plane spacing can be explained by a DIP unit cell with molecules which are slightly more upright presumably induced by a reduced grain size (see D_{coh} of DIP in Table I). Note that a similar unit cell modification was observed for submonolayers of DIP which have a similar small grain size.[33]

Grazing incidence diffraction

In addition to the XRR data, GIXD measurements were performed on the same samples. The data for the different mixing ratios prepared at different substrate temperatures are depicted in Fig. 2. The intensity of the different in-plane Bragg peaks increases with substrate temperature, as was also observed in the out-of-plane data. For the different mixing ratios, generally the Bragg peaks corresponding to the dominant material in the mixtures are more pronounced at all three substrate temperatures. The calculated values are listed in Table I for different substrate temperatures and mixing ratios.

At a substrate temperature of 303 K, the in-plane coherent crystallite size $D_{coh\|}$ is relatively small. For the equimolar mixing and the one with an excess of C_{60} only the C_{60} fcc (1 1 1) at $q_{xy} = 0.768$ $Å^{-1}$ can be fitted. Other reflections are superimposed on a wide hump in the range $q_{xy} = 1.1$–1.8 $Å^{-1}$. For a substrate temperature of 373 K, all three mixtures show well defined peaks. The size of the coherently scattering domains for both DIP and C_{60} is almost independent of the mixing ratio. Only the relative intensities of the peaks change strongly with the mixing ratio as the intensity is proportional to the amount of material in the mixtures. From the data in Fig. 2, we can clearly see that with increasing substrate temperature both the crystallinity of the pure phases as well as the degree of phase separation increase strongly. Similar to the growth of the pure materials on nSiO[46,51,52] C_{60} grows as a 3D powder,

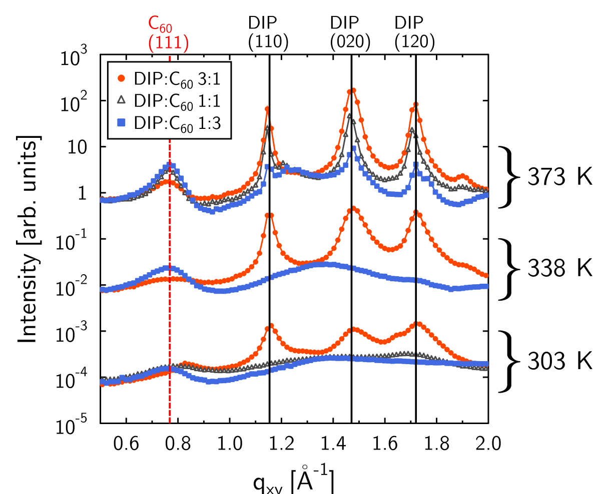

FIG. 2. GIXD of DIP:C_{60} mixtures with different mixing ratios and prepared at different substrate temperatures. Reprinted with permission from Ref. 66.

Reuse of AIP Publishing content is subject to the terms: https://publishing.aip.org/authors/rights-and-permissions. Downloaded to IP: 134.2.183.35 On: Tue, 08 Nov 2016 10:24:20

which we deduce from observing C_{60} (1 1 1) reflections both in out-of-plane as well as in in-plane scans (Figs. 1 and 2, respectively), whereas DIP domains are textured with (0 0 1) planes parallel to the sample surface.

Real-time grazing incidence diffraction

In order to investigate the evolution of the mixing behavior during film growth, real-time GIXD measurements were performed. The measurements allow us to determine the coherently scattering crystal size ($D_{coh\|}$) dependent on the film thickness during growth. Figure 3 shows an exemplary dataset for the DIP:C_{60} 3:1 mixture at a substrate temperature of 373 K. The image shows mainly the evolution of the DIP (1 1 0) and (0 2 0) peaks. For the first 4 nm the peaks are not well defined, indicating that the coherently scattering domains form only after a certain film thickness, similar to the results already reported for lower substrate temperatures.[16] In the data shown in Fig. 3, the C_{60} peak is only weakly visible, while the DIP peaks are dominant.

From the temporal evolution of the width of the Bragg peaks in the individual scans, we calculate $D_{coh\|}$ as a function of film thickness or equivalently growth time. The evolution of $D_{coh\|}$ (i) at 373 K substrate temperature is shown in Figs. 4(a)–4(c) for three different mixing ratios and (ii) at three different substrate temperatures is illustrated in Fig. 4(d) for DIP:C_{60} 3:1 mixtures.

An increase of $D_{coh\|}$ during film growth, independent of the mixing ratio, is observed at 373 K (Fig. 4). As observed from the post-growth GIXD data (Fig. 2), the absolute values of $D_{coh\|}$ for the different mixing ratios are very different. For the DIP:C_{60} 3:1 ratio, the increase of $D_{coh\|}$ of DIP is the most pronounced of all mixing ratios. We observe a very fast increase of $D_{coh\|}$ at the beginning of the growth, which saturates later (the dip at 6 nm is a fitting artefact stemming from a superposition with the C_{60} (2 2 0) peak). In contrast to this observation, for DIP:C_{60} 1:1 and 1:3 the increment in $D_{coh\|}$ as a function of thickness (for both DIP and C_{60}) is slower. For these mixing ratios, also a fast increase up to a certain thickness (~5 nm for 1:1 and ~1 nm for 1:3), followed by a rather slow increase of $D_{coh\|}$, is observed. Note that the large $D_{coh\|}$ fluctuations at the beginning of the growth ($d < 5$ nm) stem from fitting artefacts due to a weak signal at the initial stage of the growth (Fig. 4(b)).

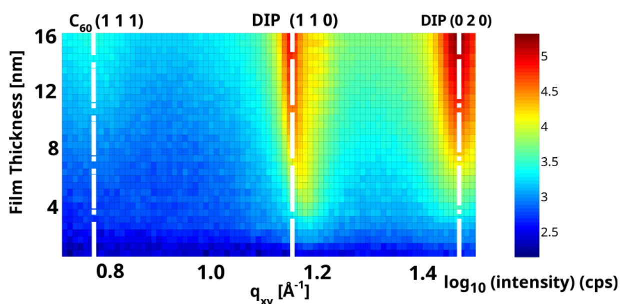

FIG. 3. Real-time GIXD data of the DIP:C_{60} 3:1 mixture prepared at 373 K. Film thickness is proportional to the growth time. Reprinted with permission from Ref. 66.

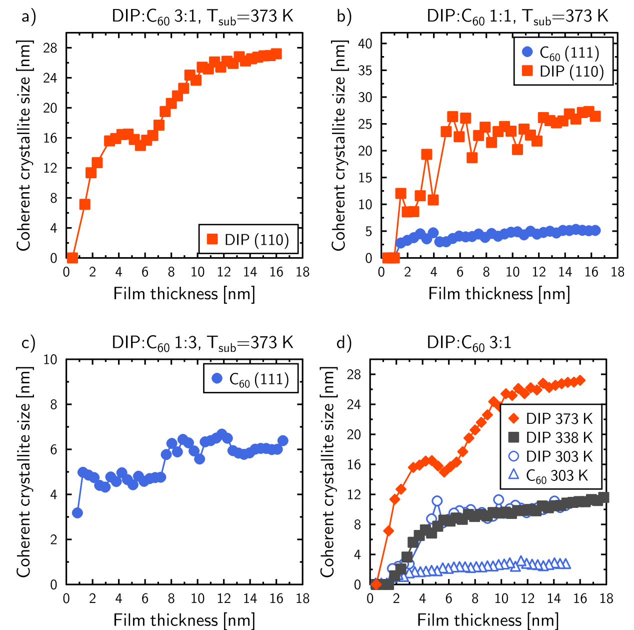

FIG. 4. Evolution of $D_{coh\|}$ of DIP:C_{60} at 373 K with the mixing ratios (a) 3:1, (b) 1:1, and (c) 1:3. (d) Evolution of $D_{coh\|}$ in DIP:C_{60} 3:1 mixtures at different substrate temperatures. Note that the strong fluctuations for a low film thickness in (b) are fitting artefacts (see text for details). Reprinted with permission from Ref. 66.

Next we focus on a comparison of the thickness dependence of $D_{coh\|}$ of DIP:C_{60} 3:1 mixtures grown at different substrate temperatures (Fig. 4(d)). With increasing substrate temperature a sudden increase of $D_{coh\|}$ is observed, which appears at lower film thicknesses. In addition, the increase of $D_{coh\|}$ during the later stage of the film growth ($d > 5$ nm) is steeper at higher substrate temperatures. However, the common observation for 3:1 mixtures at all substrate temperatures is that $D_{coh\|}$ is increasing over the whole film growth.

Real-time grazing incidence small-angle scattering

In order to characterize the evolution of the surface morphology of the mixtures, real-time GISAXS measurements were performed. A schematic of the typical GISAXS experimental setup and a typical GISAXS profile is shown in Fig. 5. Data were extracted from three different regions indicated in the image: First, the variation in intensity was monitored at the so-called anti-Bragg point of the DIP (0 0 1) peak[53] at $q_z = 0.185$ Å^{-1}, from which information on the growth mode, i.e., Frank-van der Merwe, Stranski-Krastanov, or Volmer-Weber growth, can be extracted.[27,54–56] Please note that the anti-Bragg condition of pure DIP incidentally coincides with the quarter-Bragg condition of C_{60} (1 1 1). Second, for each frame the intensity along the q_z direction in the region comprising the Yoneda wing,[57] i.e., the points in the reciprocal space map, where the exit angle equals the critical angle of the organic film (shown as a horizontal dashed line in Fig. 5), was integrated, resulting in intensity profiles along q_y. The position of the peaks stemming from the correlation of island appearing in these profiles (and also visible in the reciprocal space maps as regions of enhanced

Reuse of AIP Publishing content is subject to the terms: https://publishing.aip.org/authors/rights-and-permissions. Downloaded to IP: 134.2.183.35 On: Tue, 08 Nov 2016 10:24:20

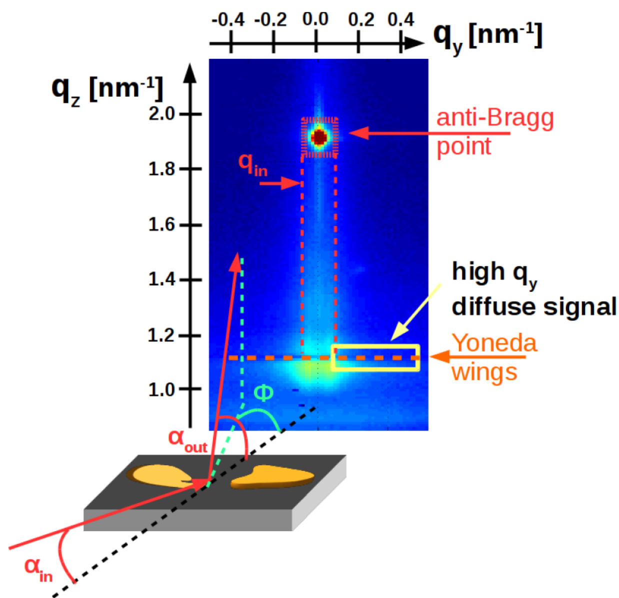

FIG. 5. Schematic of the GISAXS experiment and an example of a GISAXS real-time data acquisition. On the detector image, the regions used for the data extraction are indicated. The anti-Bragg point corresponds to a specular reflection at half of the q_z value of the DIP (0 0 1) Bragg peak. q_{in} indicates the position of an increased intensity in q_y which corresponds to D_{island}. Reprinted with permission from Ref. 66.

intensity centred along $q_y \approx \pm 0.1$ nm^{-1}) was then fitted with Lorentzians. The average island distance D_{island} was determined as $D_{island} = 2\pi/q_{cen\|}$, where $q_{cen\|}$ is the center of the peak. Furthermore, from the integrated intensity of the diffuse part of the Yoneda wing,[57] the roughness evolution of the film can be estimated.

Figure 6 depicts the different data obtained from the GISAXS profiles as a function of the film thickness for the different mixing ratios; the extracted D_{island}, the intensity of the anti-Bragg peak, and the integrated diffuse intensity is plotted. For different mixing ratios, we find different evolutions of the signals with film thickness. The gray vertical lines are used as guides for the eye. For pure DIP, the anti-Bragg oscillations match the monolayer thicknesses of standing-up DIP molecules. For all other films, the anti-Bragg oscillations obviously cannot be easily explained by the DIP material deposited alone, but complex considerations including coherent and incoherent superpositions of waves scattered from domains of different materials play a role.

The pure DIP (Fig. 6(a)) is consistent with results reported in the literature.[40,58] During the deposition of the first two monolayers, D_{island} increases rapidly to ~200 nm. From this thickness onwards, D_{island} continues to grow further up to at least ~300 nm, which is the resolution limit of the experiment. However, the well pronounced two anti-Bragg oscillations at the beginning of the growth indicate that DIP grows for the first two layers in a layer-by-layer growth mode and then the film starts to roughen quickly (damping of the anti-Bragg oscillations), as reported in Refs. 40 and 46. The diffuse signal, which is *inter alia* a measure for the roughness of the film,[59] peaks at positions of half-filled layers of the DIP film (for the first two monolayers) and afterwards increases steadily.

The blends with excess of DIP, i.e., DIP:C_{60} 3:1 and 2:1 (Figs. 6(b) and 6(c)), depict very interesting evolutions of the GISAXS signal with increasing film thickness. D_{island} increases over the whole film growth, however, not monotonously but with periodic oscillations. Both the anti-Bragg

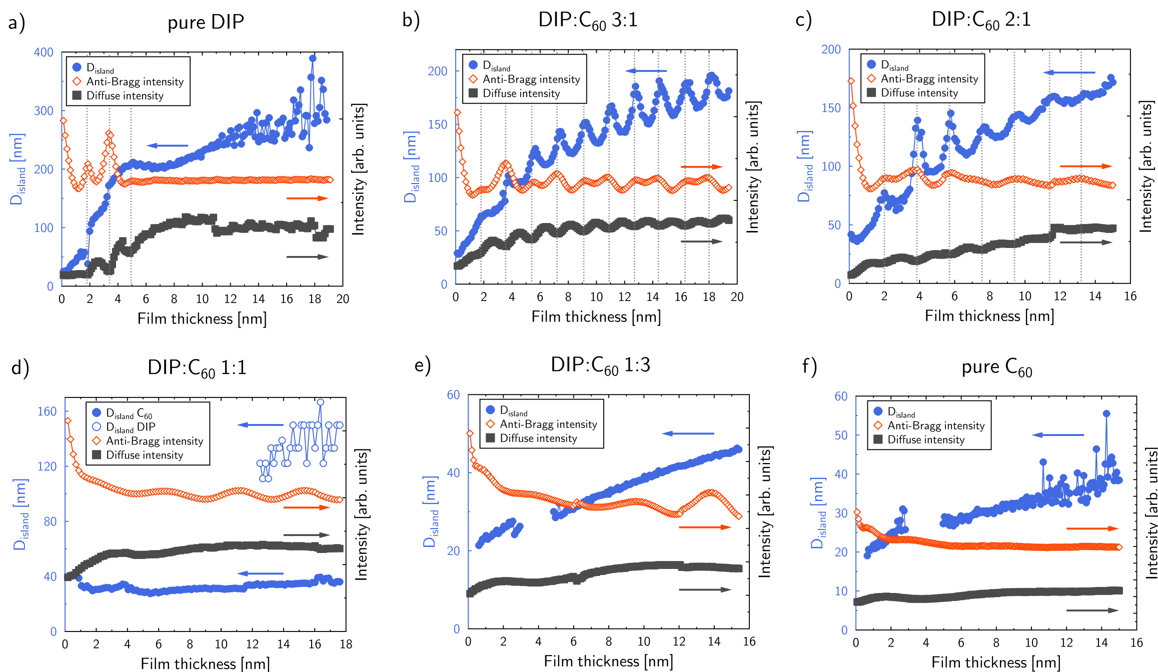

FIG. 6. Signals extracted from the real-time GISAXS measurements for different mixing ratios all prepared at 303 K. Vertical lines are used as guides for the eye to relate the positions of the local maxima in the anti-Bragg signal to the signal of the diffuse intensity and D_{island}. The diffuse intensity and the anti-Bragg intensity are vertically shifted and scaled for clarity. Note that the film thickness can be transcribed to the growth time. Reprinted with permission from Ref. 66.

Reuse of AIP Publishing content is subject to the terms: https://publishing.aip.org/authors/rights-and-permissions. Downloaded to IP: 134.2.183.35 On: Tue, 08 Nov 2016 10:24:20

as well as the diffuse intensity also show oscillations over the entire film thickness. The maxima of the diffuse intensity match positions of the minima of the anti-Bragg oscillations, which shows again that the roughness of a film has a local maximum when a layer is half-filled and is reduced afterwards. The oscillations can be observed over the whole film growth, indicating only slow roughening of the film, with the growth being close to the layer-by-layer limit. The anti-Bragg oscillations show two different periodicities and different intensity maximum values. This can be attributed to the fact that we are investigating phase-separating mixtures and non-trivial interference patterns, arising from the different materials, can be expected. Note that it is difficult to designate the maxima of the anti-Bragg oscillations to specific monolayers for mixtures, since DIP and C_{60} are sterically incompatible (ratio of long DIP axis to C_{60} diameter being ~2:1) and therefore the definition of a monolayer is not obvious.

In contrast to blends with excess DIP, the equimolar and C_{60} dominated mixtures show a different evolution of the GISAXS signals (Figs. 6(d) and 6(e)). D_{island} is clearly smaller than in the DIP dominated mixtures. Furthermore, there are neither distinct oscillations in the D_{island} evolution nor in the diffuse signal. However, the anti-Bragg intensities for the DIP:C_{60} 1:1 and 1:3 mixtures show oscillations with a periodicity of approximately 4 nm which, surprisingly, become more pronounced with increasing film thickness. In the GISAXS data of the 1:1 mixture, two different features corresponding to two D_{island} are observed for thicknesses higher than 12 nm. One of these can be related to DIP and the other to C_{60}, as already observed in post-growth measurements of the same mixture.[16] D_{island} of C_{60} can be basically determined throughout the entire growth.

The GISAXS data of pure C_{60} indicate that C_{60} does not grow in a layer-by-layer mode on nSiO, in contrast to what is observed for films on mica substrates.[20] Rather, the growth of the pure C_{60} and DIP:C_{60} 1:1 and 1:3 seems to be similar. D_{island} has a similar magnitude and time-evolution for all three films (Figs. 6(d)–6(f)). Moreover, also the roughness evolution, estimated from the evolution of the diffuse intensity, is similar. Note that for film thicknesses between 2.5 and 4.5 nm, D_{island} could not be determined for DIP:C_{60} 1:3 (and pure C_{60}), since no intensity maxima related to D_{island} were observed in the probed q_y region. In this thickness interval, we assume that the films grow again in a near-layer-by-layer mode. For C_{60} on mica thickness regions without well defined in-plane correlation peaks are also observed, which are probably related to completely filled layers.[20]

DISCUSSION

The real-time GIXD and GISAXS measurements reveal a different temporal evolution of grain sizes and surface morphologies for the different mixing ratios. For 3:1 mixtures, we observe favorable conditions for the crystallization of DIP. In addition, at 373 K we can also resolve the formation of C_{60} crystal grains. The kinetically limited phase separation reported for DIP:C_{60} 1:1 at 303 K[16] is even more pronounced in DIP:C_{60} 3:1. With increasing substrate temperature $D_{coh\|}$ increases, indicating a larger length scale of phase separation due to the enhanced thermal energy of the molecules. All measurements indicate that DIP:C_{60} forms smoother films at all investigated substrate temperatures compared to pure phase films.[46] From the real-time GISAXS data at 303 K, one can conclude a growth mode close to the layer-by-layer limit (Fig. 7(a)) accompanied by an increase of the $D_{coh\|}$ as well as of D_{island} over the whole film growth. The overall increase of island distance D_{island} with film thickness means that the average island density decreases with film thickness. For each subsequent layer, the domain size increases. The reason for this might be that a more shallow surface potential landscape exists due to the underlying organic layer that leads to larger diffusion lengths of the molecules and therefore fewer, but larger islands.[60] The observed continuous filling of the single layers leading to very smooth films might be explained by the C_{60} filling the voids between the DIP crystallites. Besides an overall increase of D_{island} with film thickness, an interesting intra-layer behavior of D_{island} is observed. At the beginning of each layer D_{island} decreases, which indicates that new islands are formed. During the further filling of the layer, the number of islands increases, leading to a further decrease of D_{island}. From a certain layer coverage onwards (a little more than 50%), the islands get very close together and start to coalesce (Fig. 7(b)). This can be seen by an increase of D_{island}. This is qualitatively different to the growth kinetics of pure DIP where after ~3 monolayers a transition to the island growth is observed.[40] Presumably, the islands in the mixtures do not consist purely of one material and the C_{60} may decorate the step-edges of the DIP, as observed for C_{60} deposited on pentacene.[61] The difference between D_{island} and $D_{coh\|}$ indicates that the islands can include both materials and are not formed by a single coherently scattering domain.

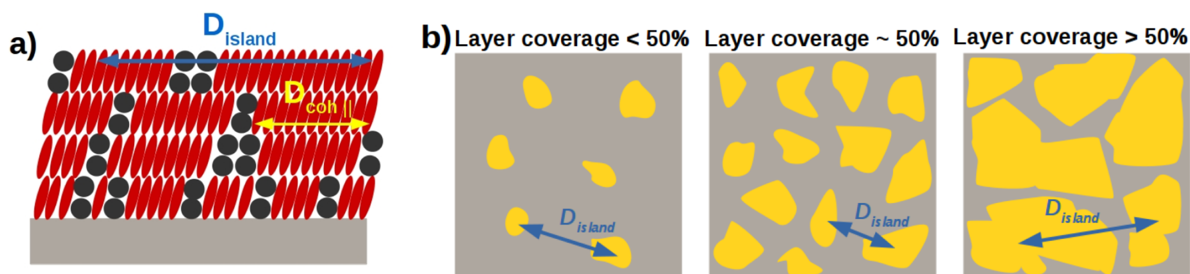

FIG. 7. Schematic of the growth of DIP:C_{60} 3:1. (a) Side view of the almost perfect layer by layer growth. (b) Top view of the growth of one layer. For a coverage less than 50%, the number of islands is increasing, resulting in a decrease of D_{island}. At ~50% merging of the islands starts, which leads again to an increase of D_{island} for coverages larger than 50%. Reprinted with permission from Ref. 66.

Reuse of AIP Publishing content is subject to the terms: https://publishing.aip.org/authors/rights-and-permissions. Downloaded to IP: 134.2.183.35 On: Tue, 08 Nov 2016 10:24:20

Most likely, impinging DIP and C_{60} molecules which arrive on the top of not completely filled layer diffuse relatively fast to the step edge and jump to the layer below to fill the voids between the islands or attach to the islands and increase the island size. The presence of C_{60} leads potentially to a reduced Ehrlich-Schwoebel barrier,[62,63] in the film. Calculations for C_{60} on the top of DIP already suggest a relatively low Ehrlich-Schwoebel barrier which C_{60} has to overcome to jump to a lower layer.[64] We conclude that the presence of DIP may facilitate the diffusion of the more prevalent C_{60} molecules down the molecular steps at the edges of islands, which results in the layer-by-layer growth mode and smoother films compared to pure C_{60}.

This is different for pure DIP where a rapid roughening of the film, which has been explained by local spatial inhomogeneities and resulting locally different growth rates[46] and strain effects,[65] has been reported. The C_{60} in the mixtures can potentially fill voids between tilted DIP domains and lead to a more homogeneous energetic landscape for molecular diffusion in further layers.

The growth of DIP:C_{60} 1:1 and 1:3 is different. There are no oscillations of D_{island} with film thickness and the almost constant diffuse signal indicates that the roughness of the films is not changing drastically during the growth, probably since the formed islands are randomly arranged on the surface and not as well ordered as observed for the DIP:C_{60} 3:1 mixture. The overall low roughness for a substrate temperature of 303 K suggests that also for these two mixtures the growth is close to a layer-by-layer mode. However, DIP and C_{60} do not form well-ordered crystallites as observed in the DIP:C_{60} 3:1 mixture. In this case, the stochastically mixed fraction of the film seems to dominate the growth.

CONCLUSION

In conclusion, we have seen that the mixing ratio has a strong impact on the growth of DIP:C_{60} mixtures. For mixtures in which DIP is the dominant part, the growth resembles the growth of pure DIP, including the formation of pure DIP crystallites, but instead of island growth,[46] we observe a pure layer-by-layer growth with a very smooth top surface. This is probably due to C_{60} molecules filling the voids between DIP crystallites. For DIP:C_{60} in the mixing ratio 3:1 prepared at a substrate temperature 303 K, the island distance D_{island} increases continuously over the whole film thickness; however $D_{coh\|}$ is increasing only very slowly, which means that there is a distinct difference between the coherently scattering domain size and the average island distance (which is related to the island size).

For higher substrate temperatures, an appreciable increase in the coherent crystal size $D_{coh\|}$ is observed, showing that the length scale of phase separation is increasing with film thickness.

On the other hand, equimolar and C_{60} dominated mixtures show a different growth scenario. The films exhibit a significant lower crystallinity and a weaker increase of $D_{coh\|}$ with film thickness. However, at 303 K also a growth mode which is close to the limit of the pure layer-by-layer growth can be expected.

ACKNOWLEDGMENTS

This work was supported by the German Research Foundation (DFG) and by the Baden-Württemberg Stiftung. C.L. thanks the Carl-Zeiss-Stiftung for funding, R.B. acknowledges funding by HYMEC, and J.N. acknowledges financial support from the project CEITEC 2020 (Grant No. LQ1601 financed by the MEYS of the Czech Republic). We also acknowledge support from DAAD/AWTR/MEYS Grant No. 57215815/7AMB16DE006.

[1] S. R. Forrest, "The path to ubiquitous and low-cost organic electronic appliances on plastic," Nature **428**, 911–918 (2004).
[2] W. Brütting and C. Adachi, in *Physics of Organic Semiconductors*, 2nd ed., edited by W. Brütting (Wiley VCH-Verlag, Weinheim, 2012).
[3] J. Lewis, "Material challenge for flexible organic devices," Mater. Today **9**, 38–45 (2006).
[4] G. Witte and C. Wöll, "Molecular beam deposition and characterization of thin organic films on metals for applications in organic electronics," Phys. Status Solidi A **205**, 497–510 (2008).
[5] J. C. Bernède, "Organic photovoltaic cells: History, principle and techniques," J. Chil. Chem. Soc. **53**, 1549–1564 (2008).
[6] H. E. Katz and J. Huang, "Thin-film organic electronic devices," Annu. Rev. Mater. Res. **39**, 71–92 (2009).
[7] B. Kippelen and J.-L. Brédas, "Organic photovoltaics," Energy Environ. Sci. **2**, 251–261 (2009).
[8] S. Ahmad, "Organic semiconductors for device applications: Current trends and future prospects," J. Polym. Eng. **34**, 279–338 (2014).
[9] W. Cao and J. Xue, "Recent progress in organic photovoltaics: Device architecture and optical design," Energy Environ. Sci. **7**, 2123 (2014).
[10] F. Schreiber, "Organic molecular beam deposition: Growth studies beyond the first monolayer," Phys. Status Solidi A **201**, 1037–1054 (2004).
[11] G. Witte and C. Wöll, "Growth of aromatic molecules on solid substrates for applications in organic electronics," J. Mater. Res. **19**, 1889–1916 (2004).
[12] A. Opitz, J. Wagner, W. Brütting, I. Salzmann, N. Koch, J. Manara, J. Pflaum, A. Hinderhofer, and F. Schreiber, "Charge separation at molecular donor-acceptor interfaces: Correlation between morphology and solar cell performance," IEEE J. Sel. Top. Quantum Electron. **16**, 1707 (2010).
[13] A. Hinderhofer and F. Schreiber, "Organic-organic heterostructures: Concepts and applications," Chem. Phys. Chem. **13**, 628–643 (2012).
[14] A. Aufderheide, K. Broch, J. Novák, A. Hinderhofer, R. Nervo, A. Gerlach, R. Banerjee, and F. Schreiber, "Mixing-induced anisotropic correlations in molecular crystalline systems," Phys. Rev. Lett. **109**, 156102 (2012).
[15] J. P. Reinhardt, A. Hinderhofer, K. Broch, U. Heinemeyer, S. Kowarik, A. Vorobiev, A. Gerlach, and F. Schreiber, "Structural and optical properties of mixed diindenoperylene-perfluoropentacene thin films," J. Phys. Chem. C **116**, 10917–10923 (2012).
[16] R. Banerjee, J. Novák, C. Frank, C. Lorch, A. Hinderhofer, A. Gerlach, and F. Schreiber, "Evidence for kinetically limited thickness dependent phase separation in organic thin film blends," Phys. Rev. Lett. **110**, 185506 (2013).
[17] J. Wagner, M. Gruber, A. Hinderhofer, A. Wilke, B. Bröker, J. Frisch, P. Amsalem, A. Vollmer, A. Opitz, N. Koch *et al.*, "High fill factor and open circuit voltage in organic photovoltaic cells with diindenoperylene as donor material," Adv. Funct. Mater. **20**, 4295–4303 (2010).
[18] A. C. Dürr, N. Koch, M. Kelsch, A. Rühm, J. Ghijsen, R. L. Johnson, J.-J. Pireaux, J. Schwartz, F. Schreiber, H. Dosch *et al.*, "Interplay between morphology, structure, and electronic properties at diindenoperylene-gold interfaces," Phys. Rev. B **68**(1–12), 115428 (2003).
[19] Y. L. Huang, W. Chen, H. Huang, D. C. Qi, S. Chen, X. Y. Gao, J. Pflaum, and A. T. S. Wee, "Ultrathin films of diindenoperylene on graphite and SiO_2," J. Phys. Chem. C **113**, 9251–9255 (2009).
[20] S. Bommel, N. Kleppmann, C. Weber, H. Spranger, P. Schäfer, J. Novak, S. Roth, F. Schreiber, S. Klapp, and S. Kowarik, "Unravelling the multilayer growth of the fullerene C_{60} in real time," Nat. Commun. **5**, 5388 (2014).
[21] S. K. Sinha, E. B. Sirota, S. Garoff, and H. B. Stanley, "X-ray and neutron scattering from rough surfaces," Phys. Rev. B **38**, 2297–2311 (1988).
[22] V. Holý and T. Baumbach, "Nonspecular x-ray reflection from rough multilayers," Phys. Rev. B **49**, 10668–10676 (1994).

Reuse of AIP Publishing content is subject to the terms: https://publishing.aip.org/authors/rights-and-permissions. Downloaded to IP: 134.2.183.35 On: Tue, 08 Nov 2016 10:24:20

[23]V. Holý, U. Pietsch, and T. Baumbach, *High-Resolution X-Ray Scattering from Thin Films and Multilayers*, Springer Tracts in Modern Physics (Springer, Berlin, 1999).

[24]J. Z. Tischler, G. Eres, B. C. Larson, C. M. Rouleau, P. Zschack, and D. H. Lowndes, "Nonequilibrium interlayer transport in pulsed laser deposition," Phys. Rev. Lett. **96**, 226104 (2006).

[25]P. Beyer, T. Breuer, S. Ndiaye, A. Zykov, A. Viertel, M. Gensler, J. P. Rabe, S. Hecht, G. Witte, and S. Kowarik, "Lattice matching as the determining factor for molecular tilt and multilayer growth mode of the nanographene hexa-peri-hexabenzocoronene," ACS Appl. Mater. Interfaces **6**, 21484–21493 (2014).

[26]A. R. Woll, T. V. Desai, and J. R. Engstrom, "Quantitative modeling of *in situ* X-ray reflectivity during organic molecule thin film growth," Phys. Rev. B **84**, 075479 (2011).

[27]B. Krause, F. Schreiber, H. Dosch, A. Pimpinelli, and O. H. Seeck, "Temperature dependence of the 2D-3D transition in the growth of PTCDA on Ag(111): A real-time X-ray and kinetic Monte Carlo study," Europhys. Lett. **65**, 372–378 (2004).

[28]T. Michely and J. Krug, *Islands, Mounds, and Atoms. Patterns and Processes in Crystal Growth Far from Equilibrium* (Springer, Berlin, 2004).

[29]J. H. Neave, P. J. Dobson, B. A. Joyce, and J. Zhang, "Reflection high energy electron diffraction oscillations from vicinal surfaces a new approach to surface diffusion measurements," Appl. Phys. Lett. **47**, 100–102 (1985).

[30]P. I. Cohen, P. R. Pukite, J. M. Van Hove, and C. S. Lent, "Reflection high energy electron diffraction studies of epitaxial growth on semiconductor surfaces," J. Vac. Sci. Technol. A **4**, 1251–1258 (1986).

[31]G. Eres, J. Tischler, M. Yoon, B. Larson, C. Rouleau, D. Lowndes, and P. Zschack, "Time-resolved study of $SrTiO_3$ homoepitaxial pulsed-laser deposition using surface x-ray diffraction," Appl. Phys. Lett. **80**, 3379–3381 (2002).

[32]S. Kowarik, A. Gerlach, W. Leitenberger, J. Hu, G. Witte, C. Wöll, U. Pietsch, and F. Schreiber, "Energy-dispersive X-ray reflectivity and for real-time growth studies of pentacene thin films," Thin Solid Films **515**, 5606–5610 (2007).

[33]S. Kowarik, A. Gerlach, S. Sellner, F. Schreiber, L. Cavalcanti, and O. Konovalov, "Real-time observation of structural and orientational transitions during growth of organic thin films," Phys. Rev. Lett. **96**(1–4), 125504 (2006).

[34]T. V. Desai, A. R. Woll, F. Schreiber, and J. R. Engstrom, "Nucleation and growth of perfluoropentacene on self-assembled monolayers: Significant changes in island density and shape with surface termination," J. Phys. Chem. C **114**, 20120 (2010).

[35]E. R. Kish, R. K. Nahm, A. R. Woll, and J. R. Engstrom, "When the sequence of thin film deposition matters: Examination of organic-on-organic heterostructure formation using molecular beam techniques and *in situ* real time x-ray synchrotron radiation," J. Phys. Chem. C **120**, 6165–6179 (2016).

[36]P. Fuoss, D. Kisker, F. Lamelas, G. Stephenson, P. Imperatori, and S. Brennan, "Time-resolved X-ray-scattering studies of layer-by-layer epitaxial growth," Phys. Rev. Lett. **69**, 2791–2794 (1992).

[37]M. V. R. Murty, T. Curcic, A. Judy, B. H. Cooper, A. R. Woll, J. D. Brock, S. Kycia, and R. L. Headrick, "Real-time X-ray scattering study of surface morphology evolution during ion erosion and epitaxial growth of Au(111)," Phys. Rev. B **60**, 16956–16963 (1999).

[38]A. Fleet, D. Dale, A. R. Woll, Y. Suzuki, and J. D. Brock, "Multiple time scales in diffraction measurements of diffusive surface relaxation," Phys. Rev. Lett. **96**, 055508 (2006).

[39]P. V. Chinta, S. J. Callori, M. Dawber, A. Ashrafi, and R. L. Headrick, "Transition from laminar to three-dimensional growth mode in pulsed laser deposited $BiFeO_3$ film on (001) $SrTiO_3$," Appl. Phys. Lett. **101**, 201602 (2012).

[40]C. Frank, J. Novák, R. Banerjee, A. Gerlach, F. Schreiber, A. Vorobiev, and S. Kowarik, "Island size evolution and molecular diffusion during growth of organic thin films followed by time-resolved specular and off-specular scattering," Phys. Rev. B **90**(4), 045410 (2014).

[41]J. Als-Nielsen and D. McMorrow, *Elements of Modern X-ray Physics*, 2nd ed. (John Wiley & Sons, Ltd., Chichester, 2011).

[42]*X-ray and Neutron Reflectivity: Principles and Applications*, Lecture Notes in Physics Vol. 58, edited by J. Daillant and A. Gibaud (Springer, Berlin, 1999).

[43]K. A. Ritley, B. Krause, F. Schreiber, and H. Dosch, "A portable ultrahigh vacuum organic molecular beam deposition system for *in situ* x-ray diffraction measurements," Rev. Sci. Instrum. **72**, 1453–1457 (2001).

[44]L. G. Parratt, "Surface studies of solids by total reflection of X-rays," Phys. Rev. **95**, 359–369 (1954).

[45]M. Björck and G. Andersson, "GenX: An extensible X-ray reflectivity refinement program utilizing differential evolution," J. Appl. Cryst. **40**, 1174–1178 (2007).

[46]A. C. Dürr, F. Schreiber, K. A. Ritley, V. Kruppa, J. Krug, H. Dosch, and B. Struth, "Rapid roughening in thin film growth of an organic semiconductor (diindenoperylene)," Phys. Rev. Lett. **90**, 016104 (2003).

[47]A. C. Dürr, F. Schreiber, M. Münch, N. Karl, B. Krause, V. Kruppa, and H. Dosch, "High structural order in thin films of the organic semiconductor diindenoperylene," Appl. Phys. Lett. **81**, 2276–2278 (2002).

[48]P. Scherrer, "Bestimmung der Größe und der inneren Struktur von Kolloidteilchen mittels Röntgenstrahlen," Nachr. Ges. Wiss. Göttingen, Math-Phys Kl. **1918**, 98–100.

[49]P. R. Willmott, D. Meister, S. J. Leake, M. Lange, A. Bergamaschi, M. Böge, M. Calvi, C. Cancellieri, N. Casati, A. Cervellino *et al.*, "The materials science beamline upgrade at the Swiss Light Source," J. Synchrotron Radiat. **20**, 667–682 (2013).

[50]S. Kowarik, A. Gerlach, M. W. A. Skoda, S. Sellner, and F. Schreiber, "Real-time studies of thin film growth: Measurement and analysis of X-ray growth oscillations beyond the anti-Bragg point," Eur. Phys. J. Spec. Top. **167**, 11–18 (2009).

[51]A. Hinderhofer, T. Hosokai, C. Frank, J. Novák, A. Gerlach, and F. Schreiber, "Templating effect for organic heterostructure film growth: Perfluoropentacene on diindenoperylene," J. Phys. Chem. C **115**, 16155 (2011).

[52]S. Kowarik, A. Gerlach, S. Sellner, L. Cavalcanti, O. Konovalov, and F. Schreiber, "Real-time X-ray diffraction measurements of structural dynamics and polymorphism in diindenoperylene growth," Appl. Phys. A **95**, 233–239 (2009).

[53]A. Dürr, B. Nickel, V. Sharma, U. Täffner, and H. Dosch, "Observation of competing modes in the growth of diindenoperylene on SiO_2," Thin Solid Films **503**, 127 (2006).

[54]J. A. Venables, *Introduction to Surface and Thin Film Processes* (Cambridge University Press, 2000).

[55]C. L. Nicklin, C. Norris, P. Steadman, J. S. G. Taylor, and P. B. Howes, "The growth of Sm on Mo(110) studied by surface X-ray diffraction," Physica B **221**, 86–89 (1996).

[56]E. Vlieg, A. W. Denier van der Gon, and J. F. van der Veen, "Surface X-ray scattering during crystal growth: Ge on Ge(111)," Phys. Rev. Lett. **61**, 2241–2244 (1988).

[57]Y. Yoneda, "Anomalous surface reflection of X rays," Phys. Rev. **131**, 2010–2013 (1963).

[58]C. Frank, R. Banerjee, M. Oettel, A. Gerlach, J. Novák, G. Santoro, and F. Schreiber, "Analysis of island shape evolution from diffuse x-ray scattering of organic thin films and implications for growth," Phys. Rev. B **90**, 205401 (2014).

[59]S. K. Sinha, "X-ray diffuse scattering as a probe for thin film and interface structure," J. Phys. III **4**, 1543–1557 (1994).

[60]C. Lorch, H. Frank, R. Banerjee, A. Hinderhofer, A. Gerlach, G. Li Destri, and F. Schreiber, "Controlling length-scales of the phase separation to optimize organic semiconductor blends," Appl. Phys. Lett. **107** (2015).

[61]T. Breuer and G. Witte, "Diffusion-controlled growth of molecular heterostructures: Fabrication of two-, one-, and zero-dimensional C_{60}-nanostructures on pentacene substrates," ACS Appl. Mater. Interfaces **5**, 9740–9745 (2013).

[62]G. Ehrlich and F. G. Hudda, "Atomic view of surface self-diffusion: Tungsten on tungsten," J. Chem. Phys. **44**, 1039–1049 (1966).

[63]R. L. Schwoebel and E. J. Shipsey, "Step motion on crystal surfaces," J. Appl. Phys. **37**, 3682–3686 (1966).

[64]J. E. Goose, E. L. First, and P. Clancy, "Nature of step-edge barriers for small organic molecules," Phys. Rev. B **81**, 205310 (2010).

[65]X. Zhang, E. Barrena, D. de Oteyza, and H. Dosch, "Transition from layer-by-layer to rapid roughening in the growth of DIP on SiO_2," Surf. Sci. **601**, 2420–2425 (2007).

[66]C. Lorch, "Influence of morphological and structural properties on organic photovoltaic cells," Ph.D. thesis, University of Tübingen, 2016.

Reuse of AIP Publishing content is subject to the terms: https://publishing.aip.org/authors/rights-and-permissions. Downloaded to IP: 134.2.183.35 On: Tue, 08 Nov 2016 10:24:20